Available online at www.sciencedirect.com
ScienceDirect
Physics Procedia 12 (2011) 230–238
Physics Procedia

LiM 2011

Metal Ablation with Short and Ultrashort Laser Pulses

Karl-Heinz Leitz[a,b]*, Benjamin Redlingshöfer[a], Yvonne Reg[c], Andreas Otto[a,b], Michael Schmidt[a,b,c]

[a]*Chair of Photonic Technologies, University of Erlangen-Nuremberg, Paul-Gordan-Straße 3, 91052 Erlangen, Germany*
[b]*Erlangen Graduate School in Advanced Optical Technologies, University of Erlangen-Nuremberg, Paul-Gordan-Straße 6, 91052 Erlangen, Germany*
[c]*Bayerisches Laserzentrum GmbH, blz, Konrad-Zuse-Str. 2-6, 91052 Erlangen, Germany*

Abstract

In laser microstructuring there is a general conflict between precision and efficiency. Short pulsed micro- and nanosecond systems generally allow high ablation rates. Yet, thermal damage of the workpiece cannot be avoided completely. Ultrafast pico- and femtosecond systems allow a higher precision, yet at lower ablation efficiency. This on the one hand can be attributed to the generally lower medium laser power of the ultrafast laser systems, on the other hand to the changed ablation mechanisms. In this contribution a comparative study of the ablation of metal with micro-, nano-, pico- and femtosecond laser pulses shall be presented.

Keywords: laser ablation of metals, short pulsed lasers, ultrafast lasers, beam-matter interaction

1. Pulsed Laser Ablation

Generally, in pulsed laser ablation the quality of the processing result is reduced by melt accretions and thermal damage of the workpiece and therefore increases with shorter pulse duration. However, ablation efficiency decreases as well. Single pulse drilling using milli- and microsecond pulses allows the production of many holes within a short time. As there is quite a big amount of melt involved in the process, the quality and reproducibility of the holes is rather low. If higher precision is needed, short and ultrashort pulses in combination with adequate drilling strategies are applied. During short pulse laser ablation only a small amount of melt occurs leading to higher accuracy. Ultrashort laser pulses even allow less thermal damage and a nearly melt free ablation, if it is worked close to ablation threshold. However, in the past the medium laser powers of ultrashort pulsed systems were not sufficient to fulfill industrial efficiency requirements [1, 2]. Only recently first attempts for the application of ultrashort laser pulses in industrial production have been reported [3, 4]. In the following a study of ablation efficiency of short and ultrashort laser pulses shall be presented. For this purpose different pulsed laser systems were applied reflecting the state of the art of available short and ultrashort pulsed beam sources.

* Corresponding author. Tel.: +49 9131 85 23239; Fax: +49 9131 85 23234
E-mail address: karl-heinz.leitz@lpt.uni-erlangen.de

doi:10.1016/j.phpro.2011.03.128

2. Ablation Models

In ablation with pulsed laser radiation, depending on the respective pulse length range, different beam-matter interaction mechanisms become dominant. For short laser pulses in the micro- and nanosecond range the ablation process is dominated by heat conduction, melting, evaporation and plasma formation (compare Figure 1 a). The energy of the laser pulse is absorbed on the surface of the workpiece and heat conduction leads to the formation of a temperature field. Depending on the achieved temperature the material is molten up, evaporates or is transferred to a plasma state. Ablation is determined by both evaporation and melt expulsion. It depends on pulse duration and pulse energy which ablation mechanism is dominant.

For ultrashort pico- and femtosecond laser pulses and the thereby related short timescales these classical descriptions of beam-matter interaction loose their validity. Due to the extreme intensities of ultrashort laser pulses, absorption is increased by nonlinear multi-photon absorption processes. Furthermore, within pico- and femtosecond timescales the energy cannot be transferred from the electron gas to the ion grid instantly. Here new thermal descriptions distinguishing between electron and grid temperature, the so called two-temperature model (compare Figure 2 b) become necessary in order to describe thermal phenomena [5, 6]. In ultrashort pulse laser ablation extreme pressures, densities and temperatures build up and accelerate the ionized material to enormous velocities. Due to the short interaction time the material cannot evaporate continuously but is transferred into a state of overheated liquid. This merges into a high pressure mixture of liquid droplets and vapor expanding rapidly (compare Figure 1 b). This mechanism is widely known as phase explosion [4, 7-9].

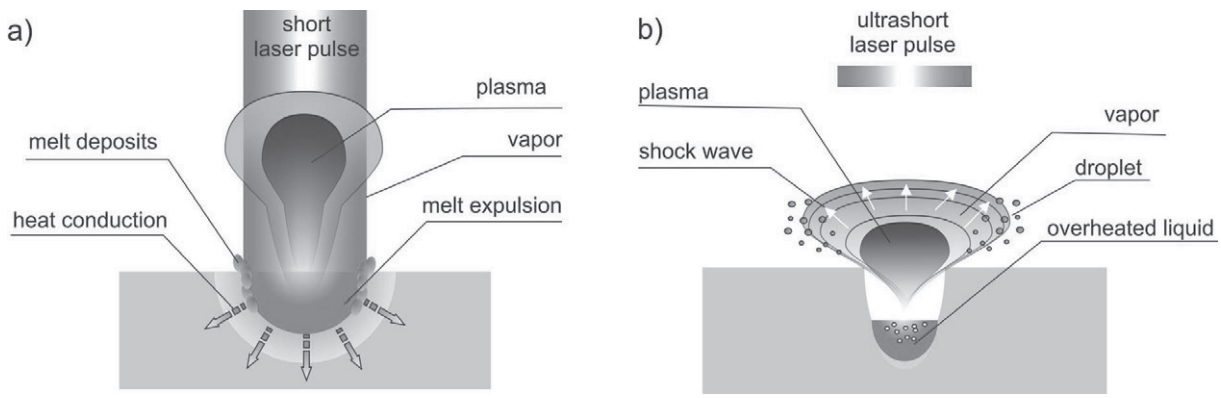

Figure 1. Beam-Matter interaction: a) classical beam-matter interaction; b) ultrafast beam-matter interaction

For the following study two ablation models were applied in order to describe the different ablation processes occurring for short and ultrashort laser pulses. The first model is based on classical beam-matter interaction. Ablation rate is estimated from energy conservation by the assumption that all the energy of the laser pulse leads to the evaporation of material. In Figure 2 a the model for classical ablation is visualized in the temperature enthalpy diagram. The energy of the laser pulse is applied in order to heat up the material to evaporation temperature and to overcome the latent heats of melting and evaporation. Material in a vapor state is ablated. The model assumes 100% energy absorption and neglects heat conduction effects as well as overheating of metal vapor:

$$m = \frac{N \cdot E_{pulse}}{c_p \cdot (T_V - T_0) + \Delta H_m + \Delta H_v} \tag{1}$$

Hereby m is the ablated mass, N the number of laser pulses, E_{pulse} the pulse energy, c_p the heat capacity, T_V evaporation temperature, T_0 ambient temperature, ΔH_m melting enthalpy and ΔH_v evaporation enthalpy.

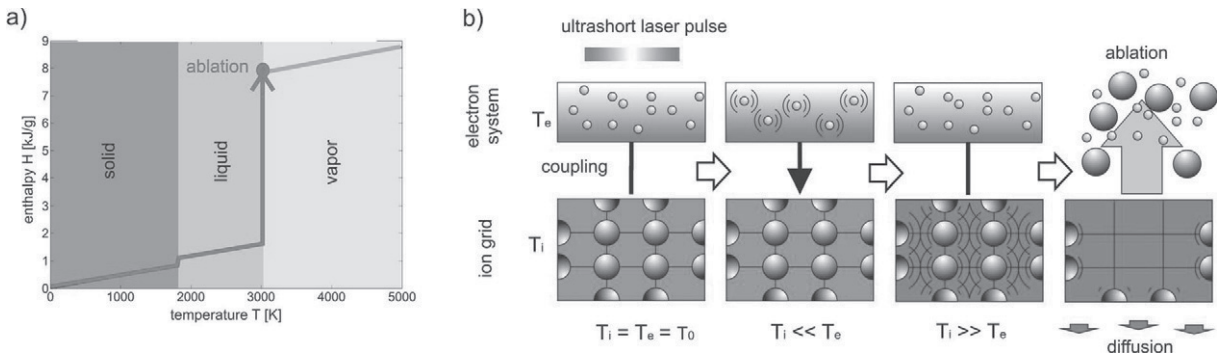

Figure 2. Ablation models: a) classical ablation model; b) two-temperature model as basis of ultrafast ablation model.

The second model is based on non-classical ultrafast beam-matter interaction. Based on the two-temperature model (compare Figure 2 b) Chichkov et al. derived a formula for ablation depth in ultrafast laser processing [5]. Based on this work ablated mass can be calculated:

$$m = N \cdot \rho \cdot A \cdot \alpha^{-1} \cdot \ln\left(\frac{F_a}{F_{th}}\right) \tag{2}$$

Hereby N is the number of laser pulses, ρ is the density, A the focal spot area, α the optical penetration depth, F_a the laser fluence and F_{th} threshold fluence for ablation.

3. Experimental Procedure

In order to study laser ablation of metal with short and ultrashort laser pulses stainless steel samples were irradiated with different numbers of mico-, nano-, pico- and femtosecond laser pulses. For this purpose different flash lamp pumped, Q-switched and mode-coupled laser systems were applied in order to reflect the bandwidth of available pulsed beam sources. The used laser systems and the respective processing parameters are listed in Table 1. The processing parameters were chosen in order to obtain maximum pulse energy and therefore ablation per pulse. They were not optimized with respect to ablation quality. The variation in peak fluence has its origin in the different processing optics of the applied systems. All the experiments were performed in air without additional process gas. The influence of process gas is investigated in [10]. The produced drillings were analyzed both qualitatively and quantitatively with scanning electron microscope and metallurgical grinding analysis with respect to traces of beam-matter interaction and ablation efficiency (ablated mass per energy).

Table 1. Applied laser systems and experimental parameters

	Microsecond laser system	**Nanosecond laser system**	**Picosecond laser system**	**Femtosecond laser system**
Model	Trumpf HL 101 P	Coherent AVIA 532-38	Time-Bandwidth Duetto	Clark-MXR CPA-1000
Wavelength λ	1064 nm	532 nm	1064 nm	800 nm
Pulse duration τ	80 µs	60 ns	10 ps	170 fs
System power P	80 W	38 W	15 W	0,7 W
Applied power P’	44 W	34 W	7,5 W	300 mW
Repetition frequency f	500 Hz	120 kHz	50 kHz	1 kHz
Pulse energy E_P	90 mJ	280 µJ	150 µJ	300 µJ
Focal spot radius r	200 µm	20 µm	40 µm	30 µm
Peak fluence F	140 J/cm²	45 J/cm²	6 J/cm²	23 J/cm²

4. Results and Discussion

Figure 3 to Figure 6 show drill holes produced with mico-, nano-, pico- and femtosecond laser pulses in different ablation stages. From the scanning electron microscope images a qualitative analysis of the ablation and beam-matter interaction process is performed. Whereas for short micro- and nanosecond pulses the ablation process is clearly thermal and dominated by classical beam-matter interaction, for ultrashort pico- and femtosecond pulses non-thermal ultrafast processes become dominant.

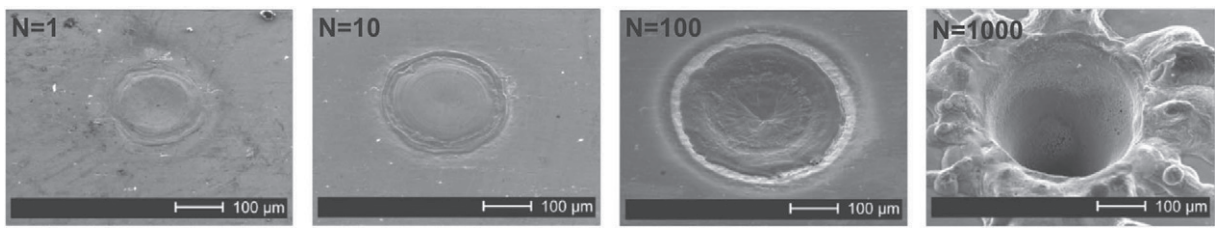

Figure 3. Laser ablation with microsecond pulses.

In the first phase the microsecond drilling process (compare Figure 3) is mainly thermal and dominated by local melting and heat conduction into the substrate. Ablation by evaporation plays a minor role. The diameter of the ablation zone steadily increases up to N=100 pulses when due to incubation effects significant ablation due to evaporation can be observed. With increasing pulse number the ablation process is more and more dominated by melt expulsion due to evaporating material manifesting itself in a pronounced burr.

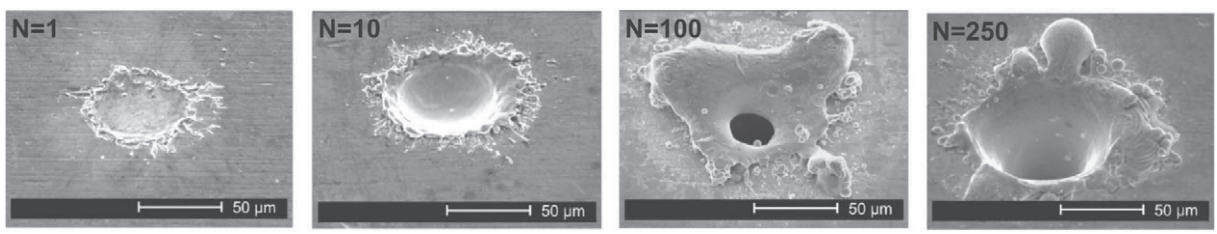

Figure 4. Laser ablation with nanosecond pulses.

The nanosecond ablation process (compare Figure 4) is still dominated by classical beam-matter interaction based on melting, evaporation and plasma formation. Yet, from the beginning evaporation and melt expulsion occur leading to a significant material removal. With increasing pulse number the diameter of the ablation zone increases. With increasing depth of the drill hole the expulsion of melt becomes less efficient leading to partly reclosure of the hole and a pronounced molten burr.

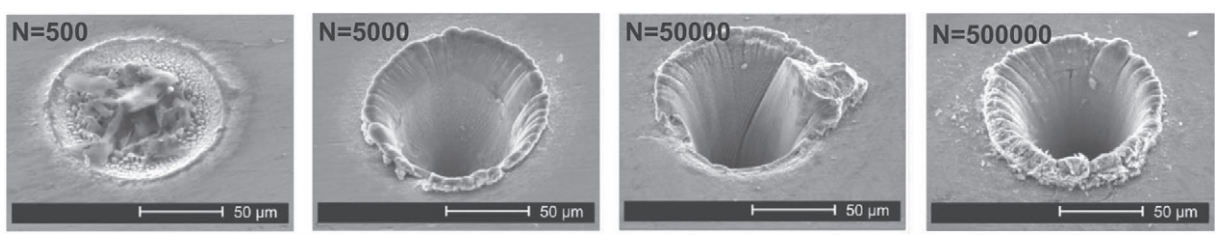

Figure 5. Laser ablation with picosecond pulses.

Due to the lower peak fluence ablation per pulse is significantly lower for the picosecond laser system (compare

Figure 5). Only a small increase in hole diameter can be observed with increasing pulse number. The cleft structure in the center of the ablation spot with N=500 pulses with deposited droplets and particles is an indicator for the occurrence of a phase explosion. In the drill holes with higher pulse numbers a soft burr of obviously molten material and ripple like structures in the deeper center of the ablation hole can be observed. The results show that for picosecond laser pulses ablation process is dominated by phase explosion. Yet, due to accumulation effects and a laser fluence far beyond ablation threshold still some thermal effects occur.

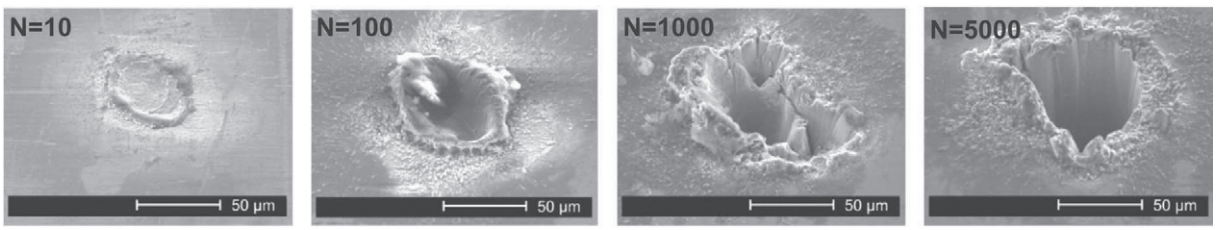

Figure 6. Laser ablation with femtosecond pulses.

For femtosecond pulses in the first phase of the ablation process ripple structures on the border of the ablation zone can be observed. The fine melt sputters show the occurrence of a phase explosion. The fact that the burr increasingly growth in height, but only slightly in width indicates that it is formed by recondensating material. With increasing pulse number burr height decreases again. Similar observations were made by Hügel et al. [11]. It can be assumed that incubation effects in combination with increased absorption at the rough surface lead to an ablation of the burr at fluences actually below ablation threshold.

For a more detailed analysis of the produced drill holes metallurgical grindings were produced. These allow both a qualitative analysis of drill hole shape and thermal influence as well as a quantitative analysis of ablation rates. Figure 7 to Figure 10 show grindings of micro-, nano-, pico and femtosecond drill holes in different stages. The grindings show different drill holes than those shown in the previous paragraph.

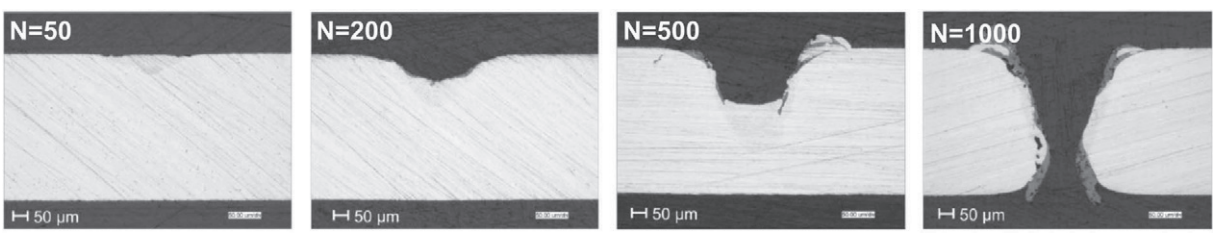

Figure 7. Drill hole evolution for microsecond pulses.

In the first phase of the microsecond pulse drilling process (compare Figure 7) nearly no ablation occurs. Instead a clear zone of local melting can be observed. Only in a later stage of the process incubation effects lead to evaporation and an ablation of material. Melt expulsion plays a minor role in the first stage of the drilling process. Furthermore, a pronounced molten zone can be observed. Only in a later stage of the drilling process, when the sheet is fully penetrated melt expulsion seems to become significant and manifests itself in a conical shape of the drill hole entrance and exit.

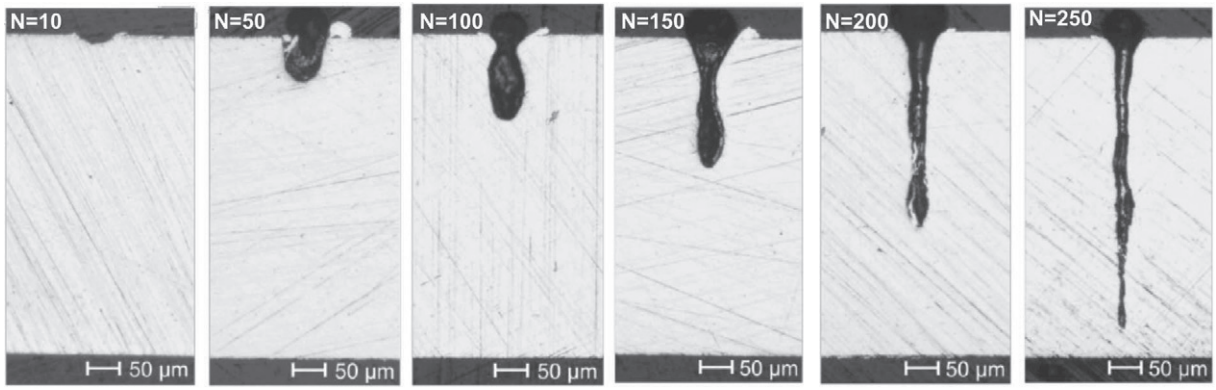

Figure 8. Drill hole evolution for nanosecond pulses.

Figure 8 shows the evolution of the drill hole for nanosecond pulses. In the first phase of the ablation process only a small burr and molten zone can be observed. The drill hole is relatively wide and shows a round shape. For N=100 and N=150 laser pulses a tapering of the drill hole can be observed. In this stage the melt expulsion efficiency decreases and a significant amount of melt remains in the drill hole. Finally this leads to a significant decrease of drill hole diameter over the hole and the drill hole becomes increasingly pointed.

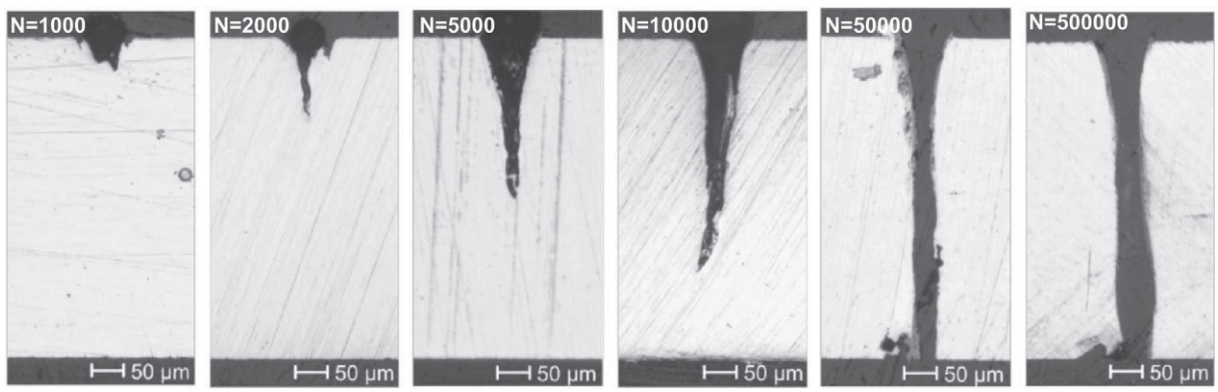

Figure 9. Drill hole evolution for picosecond pulses.

For picosecond pulses (compare Figure 9) the drill hole in the first phase is strongly cleft with several drill tips. These can be explained by scattering of the laser pulses in the ablation products of the respective previous one due to the high repetition frequency of 50 kHz. This thesis is supported by observations of König et al who observed particles above the drill hole several microseconds after the impact of a ultrashort laser pulse, making an interaction between subsequent pulses highly probable for high repetition rates [4, 12]. For higher numbers of laser pulses the drill hole becomes increasingly pointed. At N=10000 laser pulses a sickle shaped drill hole can be observed. Similar observations were made by Döring et al. during picosecond pulse drilling of silicon. He explained this effect by multiple internal reflections of the beam in the drill hole as well as interaction with particles and plasma, allowing the laser radiation to achieve shadowed areas [13, 14]. Furthermore, for N=10000 pulses melt disposals in the drill hole can be observed showing that for fluences far above ablation threshold picosecond ablation is still a partly thermal process. After full penetration a widening of the drill hole can be observed. This can be deduced to accumulation effects in combination with multiple reflections and scattering as well as by an erosive effect of the generated plasma.

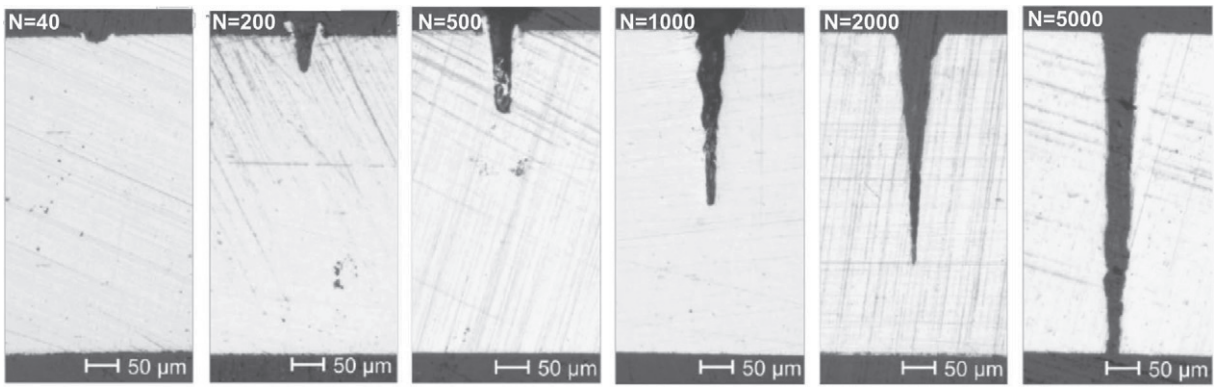

Figure 10 Drill hole evolution for femtosecond pulses.

In the first phase of the femtosecond drilling process (compare Figure 10), up to N=500 laser pulses, the drill hole has rather steep edges and the bottom shows a hemispherical shape. This can be explained by the Gaussian beam profile of the laser. Furthermore, a very steep and thin burr can be observed that can only be formed by recondensating material. In a later phase of the drilling process this burr vanishes again. Similar observations were made by Michalowski et al. who explained the vanishing of the burr by shock waves due to plasma expansion [15]. Besides in this later drilling stage the drill hole becomes increasingly pointed and shows wavy walls. The pointed shape can be deduced to multiple reflections and interference effects whereas the bulges at the walls are probably caused by the erosive effect of the generated plasma.

Besides the so far presented qualitative analysis of the ablation process and drill hole evolution the metallurgical grindings were analyzed quantitatively with respect to ablated mass. For this purpose it was assumed that the grinding shows the middle of the drill hole and that each cross section of the drill hole is perfectly circular. The obtained ablated masses are plotted in Figure 11. In order to show and compare all the experimental data in one diagram, a double logarithmic scale was chosen. Besides the experimental data theoretical curves based on the analytical models described in section 2. are plotted in Figure 11. For the calculation the parameters listed in Table 1 were used.

Table 1. Parameters used for theoretical curves [1, 9, 16]

Physical constant	**value**	**unit**
Heat capacity c_p	450	$Jkg^{-1}K^{-1}$
Evaporation temperature T_V	3133	K
Ambient temperature T_0	293	K
Melting enthalpy ΔH_M	270	$kJkg^{-1}$
Evaporation enthalpy ΔH_V	6100	$kJkg^{-1}$
Density iron	7015	kgm^{-3}
Optical penetration depth α – ps	4	nm
Threshold fluence F_{th} – ps	1	Jcm^{-2}
Optical penetration depth α – fs	20	nm
Threshold fluence F_{th} – fs	1,25	Jcm^{-2}

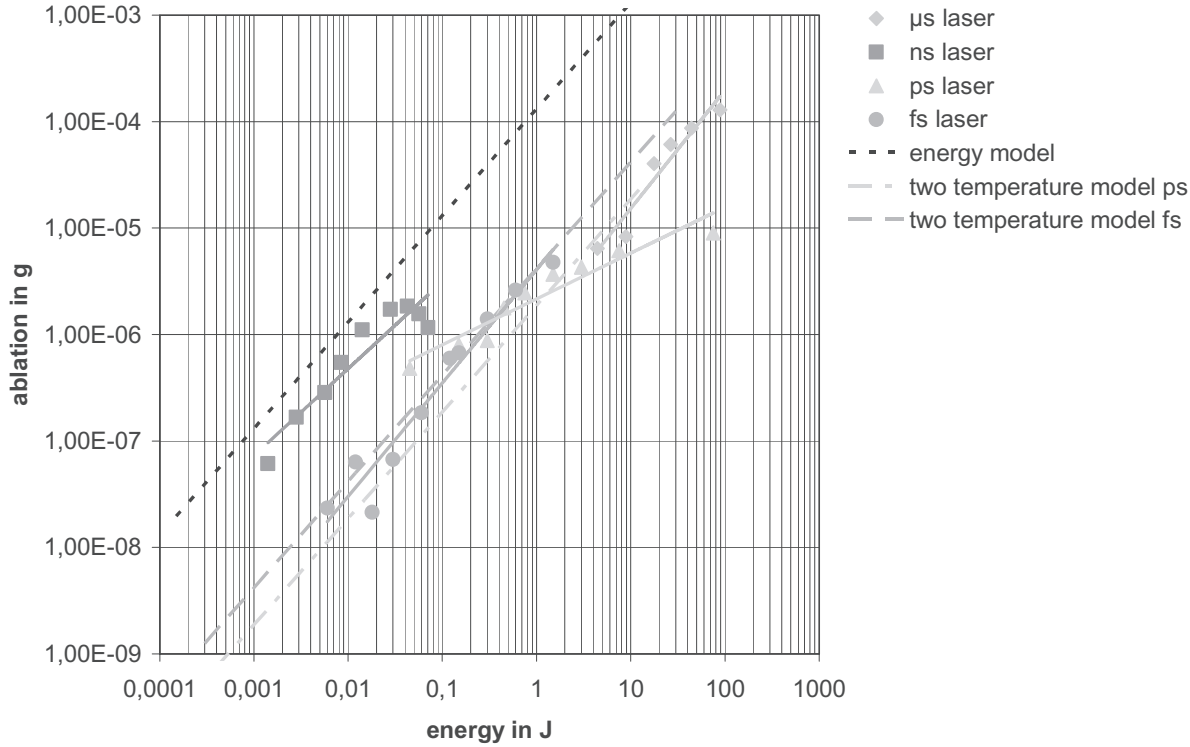

Figure 11. Ablation vs. energy for micro-, nano-, pico- and femtosecond laser pulses.

The graphs clearly show that of the investigated laser systems, the nanosecond one delivers highest ablation efficiency per applied energy. The experimental data fits quite well the theoretical curve obtained from the energy model based on equation (1). The fact that the experimental data is slightly below the theoretical curve might have its reason in the fact that absorption is below 100 % and that material is heated above evaporation temperature. Obviously the nanosecond ablation process can be described quite well by the assumption that all the energy goes into the evaporation of the material. The effects of overheating of the vapor and the expulsion of molten material that are not considered in the described strongly simplified model based on energy conservation seem to balance one another.

The ablation rate of the microsecond pulses is far below theoretical expectations from the energy model. This shows that for microsecond pulses heat conduction losses play a significant role. This effect is significantly enhanced by the low repetition rate of the microsecond pulsed system applied in the experimental study.

For femtosecond pulses the experimental data nearly perfectly fits the theoretical curve obtained from the two-temperature model based on equation (2). Corrections of optical penetration depth used by other authors for high laser fluences were not considered in the theoretical curve [9, 17]. They would lead to a slight shift of the curve in positive y-direction.

The picosecond data however shows a significantly reduced slope compared to the other curves. This cannot solely be explained by a dependency of penetration depth and threshold fluence on the respective processing parameters described by Schmid et al. in [16]. Therefore, we assume that the significantly reduced ablation efficiency of the picosecond system has its origin in particle shielding effects due to the relatively high repetition rate of 50 kHz. A comparision with the data obtained for nanosecond pulse ablation at a pulse repetition rate of 120 kHz indicates that particle shielding effects are more dominant for pico- than for nanosecond pulses. Yet, due to the difference in both fluence and optical wavelength no clear statement can be made. Here further investigations are required.

5. Conclusions

The presented results show that the ablation process of metals is significantly influenced by the pulse duration of the applied laser source and the respective processing parameters. Among the investigated laser systems the nanosecond one allows highest ablation efficiency per energy as the material is barely overheated. The nanosecond ablation process can be accurately described by a model based on the assumption that the laser energy is used for evaporation of the ablated material. The ablation rate of the pico- and femtosecond system are significantly lower. The ablation behavior of femtosecond pulses can be described based on the two-temperature model. Due to the high repetition rate of the picosecond system particle shielding effects seem to play a significant role. Due to the high medium power of the microsecond system it delivered highest ablated volumes. Yet, due to the low pulse repetition rates of the applied system heat conduction losses became dominant leading to ablation rates not higher than for the ultrafast systems.

Acknowledgements

The authors gratefully acknowledge funding of the project “Gezielte lokale Sub-100-nm-Strukturierung durch ultrakurze Laserpulse mithilfe von mit einer optischen Pinzette positionierten Kolloiden unter Ausnutzung von Nahfeldeffekten” within the DFG priority programme 1327 “Optisch erzeugte Sub-100-nm Strukturen für biomedizinische und technische Applikationen” and the funding of the Erlangen Graduate School in Advanced Optical Technologies (SAOT) by the German National Science Foundation (DFG) in the framework of the excellence initiative.

References

[1] A. Ruf, Modellierung des Perkussionsbohrens von Metallen mit kurz- und ultrakurzgepulstenLasern, in, Universität Stuttgart, 2004.
[2] K.-H. Leitz, H. Koch, A. Otto, M. Schmidt, A 3D Transient Numerical Model of Solid, Liquid and Gas Phase during Laser Beam Drilling with Short Pulses, in: A. Ostendorf, T. Graf, D. Petring, A. Otto (Eds.) Fifth International WLT-Conference on Lasers in Manufacturing, Munich, 2009, pp. 787-792.
[3] P. Trechow, Ultrakurze Laserpulse lassen Moleküle kollabieren, in: VDI Nachrichten, 2008, pp. 3.
[4] J. König, T. Bauer, Fundamentals and industrial applications of ultrashort pulsed lasers at Bosch, in: Photonics West, San Fransisco, 2011, pp. 7925-7932.
[5] B.N. Chichkov, C. Momma, S. Nolte, A. Alvensleben, A. Tünnermann, Femtosecond, picosecond and nanosecond laser ablation of solids, Appl. Phys. A, 63 (1996) 109-115.
[6] M. Dirscherl, Ultrakurzpulslaser - Grundlagen und Anwendungen, 2005.
[7] A. Miotello, R. Kelly, Laser-induced phase explosion: new physical problems when a condensed phase approaches the thermodynamic critical temperature, Appl. Phys. A, 69 (1999) 67-73.
[8] Q. Lu, S.S. Mao, X. Mao, R.E. Russoa, Delayed phase explosion during high-power nanosecond laser ablation of silicon, APPLIED PHYSICS LETTERS, 80 (2002) 3072-3074.
[9] P.T. Mannion, J. Magee, E. Coyne, G.M. O'Connor, T.J. Glynn, The effect of damage accumulation behaviour on ablation thresholds and damage morphology in ultrafast laser micro-machining of common metals in air, Applied Surface Science, 233 (2004) 275-287.
[10] Y. Reg, K.-H. Leitz, M. Schmidt, Influence of processing gas on the ablation quality at ns-laser beam ablation, in: Lasers in Manufacturing, Physics Procedia, Munich, 2011.
[11] H. Hügel, T. Graf, Laser in der Fertigung, 2 ed., Vieweg+Teubner, 2009.
[12] J. König, S. Nolte, A. Tünnermann, Plasma evolution during metal ablation with ultrashort laser pulses, OPTICS EXPRESS, 13 (2005) 10597-10607.
[13] S. Döring, S. Richter, S. Nolte, A. Tünnermann, In situ imaging of hole shape evolution in ultrashort pulse laser drilling, OPTICS EXPRESS, 18 (2010) 20395-20400.
[14] S. Döring, S. Richter, S. Nolte, A. Tünnermann, In-situ observation of the hole formation during deep drilling with ultrashort laser pulses, in: Photonics West, 2011, pp. 7920-7939.
[15] A. Michalowski, R. Weber, T. Graf, Diagnostic studies of melt transport during ultrashort pulse laser drilling, in: WLT-Conference on Lasers in Manufacturing, Munich, 2009, pp. 793-797.
[16] M. Schmid, B. Neuenschwander, V. Romano, B. Jaeggi, U.W. Hunziker, Processing of metals with ps-laser pulses in the range between 10ps and 100ps, in: Photonics West, San Fransisco, 2011, pp. 7920-7908.
[17] S. Nolte, C. Momma, H. Jacobs, A. Tünnermann, B.N. Chichkov, B. Wellegehausen, H. Welling, Ablation of metal by ultrashort laser pulses, J. Opt. Soc. Am. B, 14 (1997) 2716-2722.